Fabrication of carboxymethyl cellulose/hyaluronic acid/polyvinylpyrrolidone composite pastes incorporation of minoxidil-loaded ferulic acid-derived lignin nanoparticles and valproic acid for treatment of androgenetic alopecia

Peixin Li [a,b], Yanfang Sun [c], Lei Nie [d], Amin Shavandi [e], Khaydar E. Yunusov [f], Yinjian Hua [a,b], Guohua Jiang [a,b,*]

[a] *School of Materials Science and Engineering, Zhejiang Sci-Tech University, Hangzhou, 310018, China*

[b] *International Scientific and Technological Cooperation Base of Intelligent Biomaterials and Functional Fibers, Hangzhou, 310018, China*

[c] *College of Life Sciences and Medicine, Zhejiang Sci-Tech University, Hangzhou, 310018, China*

[d] *College of Life Sciences, Xinyang Normal University, Xinyang 464000, China*

[e] *Université libre de Bruxelles (ULB), École polytechnique de Bruxelles, 3BIO-BioMatter, Avenue F.D. Roosevelt, 50 - CP 165/61, 1050 Brussels, Belgium*

[f] *Institute of Polymer Chemistry and Physics, Uzbekistan Academy of Sciences, Tashkent, 100128, Uzbekistan*

Abstract: Androgenetic alopecia (AGA) is a transracial and cross-gender disease worldwide with a higher prevalence among young individuals. Traditional oral or subcutaneous injections are often used to treat AGA, however, they may cause severe side-effects and therefore effective treatments for AGA are currently lacking. In this work, to treat AGA, we developed a composite paste system based on minoxidil (MXD)-loaded nanoparticles and valproic acid (VPA) with the assistance of roller-microneedles (roller-MNs). The matrix of composite paste systems is carboxymethyl cellulose (CMC), hyaluronic acid (HA) and polyvinylpyrrolidone (PVP). The roller-MNs can create microchannels in the skin to enhance drug transdermal efficiency. With the combined effects of the stimulation hair follicle (HF) regrowth by upregulating Wnt/beta-catenin of VPA and the mechanical microchannels induced by roller-MNs, the as-prepared composite paste systems successfully boost perifollicular vascularization, and activate hair follicle stem cells, thereby inducing notably faster hair regeneration at a lower administration frequency on AGA mouse model compared with minoxidil. This approach offers several benefits, including the avoidance of efficacy loss due to the liver's first-pass effect associated with oral drug, reduction in the risk of infection from subcutaneous injection, and significant decrease in the side effects of lower-dose MXD.

Keywords: Minoxidil, valproic acid, androgenetic alopecia, roller-microneedles, hair regeneration

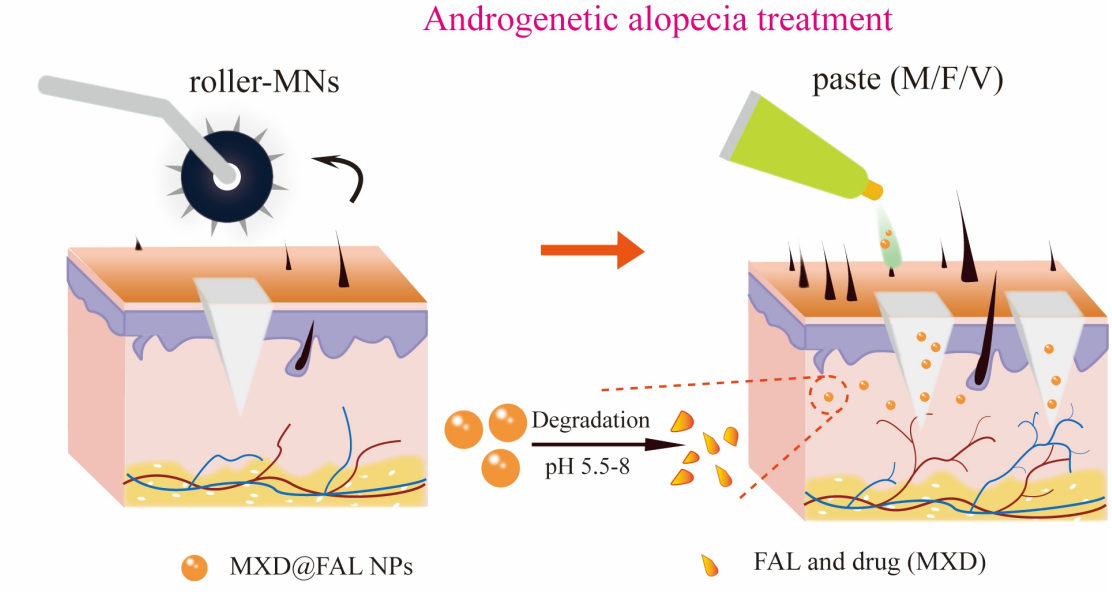
Androgenetic alopecia treatment
roller-MNs
paste (M/F/V)
Degradation
pH 5.5-8
MXD@FAL NPs
FAL and drug (MXD)

1. Introduction

Androgenetic alopecia (AGA) is the most prevalent type of alopecia areata, a condition in which the rate of hair loss exceeds the rate of hair growth and the number of hairs declines with an upward shift in the hairline [1-3]. There is a promising market for hair regrowth because of the rise in the number of people experiencing hair loss and the necessity of hair renewal [4-6]. Although there are two therapy options of follicular transplantation and medication, there is still a notable absence of convenient delivery system and an efficient treatment approach [7-10]. The US Food and Drug Administration (FDA) has only approved finasteride (FIN) and minoxidil (MXD) as medications for treating hair loss [11-14]. Although MXD, has shown positive results in treating hair loss, individuals who use MXD topically may be more prone to experiencing skin side effects and developing hypertrichosis [15-20]. Therefore, it is worth investigating alternative therapies with fewer or no side effects [21-23].

Valproic acid (VPA), an FDA-approved anticonvulsant, has been demonstrated to induce hair follicle (HF) regeneration by upregulating Wnt/b-catenin [24]. It has been reported that Wnt/β-catenin signaling is critical for the development and inductive potential of dermal papilla cells (DPC) for HF regeneration and hair shaft growth [25]. As a therapeutic agent, precise dosing of MXD and VPA is crucial to prevent adverse reactions [24,26,27].

The preferential deposition of drugs in hair follicles is determined by the physicochemical properties of the drug itself and the type of drug delivery method [28,29]. Many drug delivery systems, including polymeric carriers, lipid nanoparticles,

and microneedles (MNs), have been broadly investigated to enhance the specific delivery of active pharmaceutical ingredients to hair follicles [30]. MNs are a painless administration method that offers several advantages, including convenient usage, minimally invasive procedure, and relatively low cost. They effectively overcome the stratum corneum barrier, enabling pharmaceuticals to penetrate both epidermal and dermal layers [31]. However, the application of the MNs is limited due to the need for multiple dosing frequencies and unstable efficacy [32-35]. Wang et al [36] showed a rapid onset of therapeutic action in a xylene-induced acute inflammation model in mice by building a supramolecular dissolving microneedle patch. In contrast to supramolecular MNs [36] and polymer MNs [37-38], roller-MNs are more suitable for creating the channels in the hair-covered area. Therefore, we hypothesize that nanocarrier-integrated MNs can not only alleviate the adverse effect associated with therapeutic agents but also promote drug delivery. This synergistic approach has the potential to significantly improve the efficiency of AGA treatment [39-41].

Ferulic acid (FA) can self-assemble into lignin nanoparticles and can be applied to encapsulate drugs. Lignin nanoparticles have good biocompatibility and antioxidant characteristics [42-45]. Zhao et al [45] effectively built a lignin-derived nanoparticle loaded with cyclosporin for the treatment of inflammatory bowel disease and demonstrated efficient drug loading as well as scavenging characteristics of the nanoparticles of reactive oxygen species (ROS). Hydrophobic drugs can easily penetrate the skin barrier due to the hydrophobic and lipophilic nature of the skin's stratum corneum [46-48]. However, they usually require to be dissolved in organic

solvents, which may harm the skin [49-53].

Herein, a composite paste system with the incorporation of MXD-loaded FA-derived lignin nanoparticles (MXD@FAL NPs) and VPA was designed for the treatment of AGA with the assistance of roller-microneedles (roller-MNs). The hydrophobic MXD was encapsulated in the ferulic acid-derived nanocarriers, which overcame the insolubility problem of the lipophilic drug in the composite paste fabrication process. Using the inherent roller-MNs function that overcomes the skin barrier properties, the encapsulated MXD@FAL NPs and VPA were physically penetrated and implanted inside the skin [54-59]. CMC, HA and PVP were selected as the matrix of composite paste due to their excellent biocompatible, biodegradation, and rapid dissolution in the skin's extracellular fluid, leading to improve the permeation of the drugs [60-61]. In addition, the hair growth promotion effect of the composite pastes incorporating MXD@FAL NPs and VPA (M/F/V) was evaluated on the C57BL/6J mice (Fig. 1).

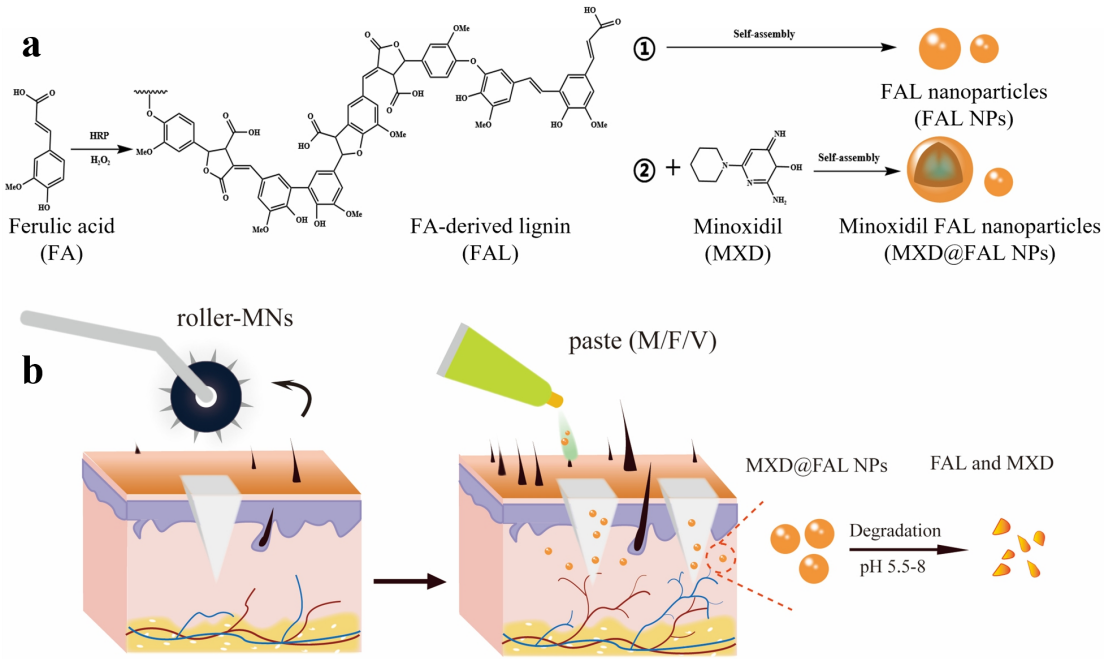

Fig. 1 Schematic illumination of composite pastes incorporation of MXD-loaded nanoparticles (MXD@FAL NPs) and valproic acid (VPA) composite paste for the treatment of androgenetic alopecia.

2. Experimental section

2.1 Materials

Minoxidil (MXD, >98.0%), valproic acid (VPA, >98.0%), ferulic acid (FA, >99.0%), carboxymethyl cellulose sodium (CMC, 1500-3100 mPa.s), hyaluronic acid (HA, 95%), polyvinylpyrrolidone (PVP, K30), phosphate buffered saline (PBS), TWEEN®80 and peroxidase from horseradish (active > 300 units/mg) were obtained from Aladdin Chemical Reagent Co., Ltd. (Shanghai, China). Hydrochloric acid (HCl), acetone, hydrogen peroxide (H_2O_2) and tetrahydrofuran (THF) were purchased from Hangzhou Shuanglin Chemical Reagent Co., Ltd. (Hangzhou, China). Dihydroethidium (DHE) and dihydrotestosterone (DHT) were purchased from Beyotime Biotechnology (Shanghai, China). DMEM was purchased from Procell Life Science&Technology Co., Ltd.

2.2 Preparation of FAL NPs and MXD@FAL NPs

Horseradish peroxidase (5 mg) was first dissolved in PBS (100 mL, pH = 8). After adding the solution of FA [FA (1 g) in 25 mL of water and acetone (4:1, v/v)] and H_2O_2 (25 mL, 1.8 wt%), the solution was further stirred for 48 h in the dark. Then, the pH of the solution was adjusted to 3 with the addition of the HCl solution. The FA-derived lignin (FAL) could be obtained after centrifuging and rinsing by deionized water.

FAL (10 mg) was dissolved in THF (10 mL). Deionised water (180 mL) was

slowly added to the stirred FAL solution at a rate of 120 mL/h. After stirring for 1 h at room temperature, the solution was centrifuged at 10,000 rpm for 6 min at 8 °C. Then, the solid composition was dialyzed (MWCO = 8,000 Da) against deionised water for 48 h. The FAL NPs were obtained after freeze-drying. For the preparation of MXD@FAL NPs, FAL (20 mg) and MXD (10 mg) were dissolved in THF (20 mL). Deionised water (200 mL) was added with a rate of 180 mL/h. Then, the mixture was stirred under room temperature for 1 h. The solvent and un-loaded drug were eliminated by centrifugation. Finally, MXD@FAL NPs were obtained by a dialysis and freeze-drying process.

2.3 Characterization

The particle size and zeta potential of samples were determined by a dynamic light scattering instrument (DLS, Zetasizer Nano ZS90) at room temperature. The morphologies of the as-obtained samples were characterized by a field emission scanning electron microscope (FE-SEM, Vltra55, Zeiss) at an extra high tension of 5 kV and transmission electron microscopy (FE-TEM, JEM-1400Flash) operated at an acceleration voltage of 120 kV. The composition of the resultant samples was analysized by an Infrared spectrometer (FT-IR, TENSOR-27). The loading efficiency and encapsulation percentage of samples were measured by an UV-Vis spectrophotometer (U3900H, Japan).

2.4 Preparation of the composite paste (M/F/V)

CMC (0.96 g), HA (0.2 g) and PVP (0.5 g) were firstly dispersed in 13.34 mL distilled water to prepare blank composite paste. Then, MXD@FAL NPs (0.1 g) and

VPA (0.4 mL) were dispersed in the above blank pastes (19.5 g) to prepare the low-dose drug composite paste (L-M/F/V). 0.4 g MXD@FAL NPs and 0.4 mL VPA were dispersed in the 19.2 g blank pastes to prepare the high-dose drug composite paste (H-M/F/V) (Table S1).

2.5 Drug release *in vitro*

The dialysis bag method (MWCO = 14,000 Da) was utilized to simulate *in vitro* drug release of composite paste (H-M/F/V). 0.3 g paste (H-M/F/V) was submerged in 30 mL of PBS containing 2.5 % Tween 80 and placed in a 37 °C water bath for 24 h (pH = 5-8). The total amount of released drug was determined by an UV-Vis spectrophotometer.

Transdermal tests were performed on the Franze diffusion cell method. Rat skin was sliced and glued to the diffusion pool with PBS that contained 30 % ethanol as the receiving medium. The effective transdermal area was 2 cm^2 and the receiving cell volume was 15 mL. Firstly, roller-MNs were used to roll over the skin 3~5 times to ensure sufficient microchannels formed on the skin surface (Table S2). And 0.3 g composite paste (H-M/F/V) was subsequently spread on the rat skin. Then, 1.5 mL samples were taken at intervals of time from receiving cell. These samples were promptly replaced with an equal volume of the same receiving medium. The total amount of released drug was determined by an UV-Vis spectrophotometer (Table S3). The transdermal test of composite paste (2% MXD) was tested at the same conditions according to the above method.

2.6 Cytotoxicity tests and androgenetic alopecia management *in vivo*

The cytotoxicity of the composite pastes was tested by culturing L929 cells using the tetrazolium-based colorimetric assay (MTT) analysis. The hair regeneration capabilities of composite pastes were evaluated in male C57BL/6 mice (6 weeks old, Zhejiang Ying Yang Pharmaceutical R&D Co., Ltd., Hangzhou, China) that followed a previous report with slight modification [23]. All the animal procedures were approved by the Animal Ethics Committee of Zhejiang Sci-Tech University (No: 202303012) and Zhejiang Yingyang Pharmaceutical R&D Co., Ltd. (No: ZJEY-20221128-04). A 4 cm^2 area (2 cm × 2 cm) of the hair from the dorsal portion of the 7-week-old mice in the telogen phase was gently shaved with an electric hair clipper and depilated with hair-removing cream. The mice were randomly divided into 7 groups (Table S4): the blank group (G1: healthy after hair removal), the control groups (G2: AGA mice treated by roller-MNs; G3: treated by blank composite paste), the minoxidil group (G4: treated by 2 % MXD composite paste), the valproic acid group (G5: treated by 2 % VPA composite paste), the L-M/F/V group (G6: treated by 0.5 % MXD@FAL NPs and 2 %VPA composite paste), and the H-M/F/V group (G7: treated by 2 % MXD@FAL NPs and 2 %VPA composite paste). A roller-MNs was applied on shaved skin to create microchannels before spreading of the composite paste (~0.15 g/cm^2). Digital pictures of skin and hair were taken at interval time. The diameter and density of regrown hair were measured with the assistance of Firefly tri-scope DE337T (Belmont, USA) at day 12 post depilation.

2.7 Histology and immunohistochemistry analysis

The hair regrowth of AGA C57BL/6J mice was assessed by hematoxylin and

eosin staining (H&E). Inflammation at the hair regrowth area was evaluated by interleukin 6 (IL-6). The level of reactive oxygen species (ROS) at the hair regrowth area was determined by fluorescence DHE.

2.8 Statistical analysis

The statistical analysis was performed using the statistical software GraphPad Prism 7. Student's t test and one-way analysis of variance were used for statistical comparison. A p-value < 0.05 was considered statistically significant. (∗P < 0.05, ∗∗P < 0.01, ∗∗∗P < 0.001, ∗∗∗∗P < 0.0001)

3. Results and discussion

3.1 Synthesis and Characterization of FAL NPs and MXD@FAL NPs

The morphology of FAL NPs is confirmed by SEM and TEM tests. As shown in Fig. 2a, the spherical structure of FAL NPs can be observed from the SEM image. The intra/intermolecular π-π stacking interactions of aromatic rings govern the formation of the spherical structure of FAL NPs [62]. In addition, the FAL NPs tend to aggregate due to the hydrogen bonding or van der Waals interaction, as shown in Fig. 2b. Fig. 2c shows the particle size distribution of FAL NPs, ranging from 200 to 400 nm. Because of the abundant aliphatic hydroxyl group of FAL, the hydrophobic minoxidil (MXD) can be incorporated into the FAL NPs through a hydrophobic interaction. As shown in Fig. 2d, spherical morphology still can be maintained after loading of MXD. And core-shell structure of MXD@FAL NPs can be observed from the TEM image (Fig. 2e). The size of MXD@FAL NPs is 300-600 nm and confirmed by the DLS test (Fig. 2f). Due to the excellent physicochemical properties including antibacterial and

antioxidant, lignin-based composites is a suitable candidate for drug delivery applications [63].

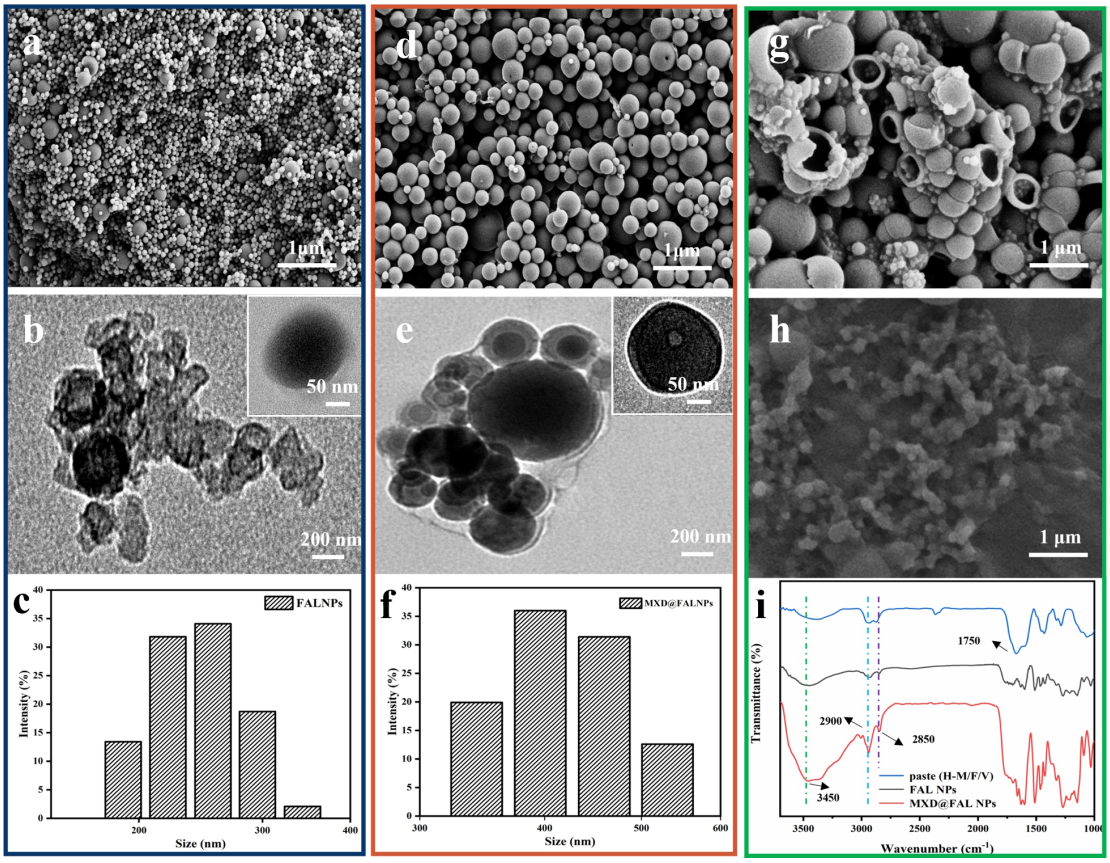

Fig. 2 The morphology and composition of FAL NPs, MXD@FAL NPs and composite paste. SEM (a), TEM (b) images and particle size distribution (c) of FAL NPs, SEM (d), TEM (e) images and particle size distribution (f) of MXD@FAL NPs, SEM (g and h) images of MXD@FAL NPs in PBS with pH = 6.5 for 2 and 6h, and FTIR spectra (i) of FAL NPs, MXD@FAL NPs and composite paste (H-M/F/V).

Herein, the stability of MXD@FAL NPs in PBS solution is also evaluated after incubation for 2 h. As shown in Fig. 2g, the structural integrity of MXD@FAL NPs has been destroyed. Further increasing incubation time to 6 h, the spherical structure of MXD@FAL NPs is disappeared (Fig. 2h). It indicates that lignin-based carriers can be degraded which is beneficial for drug release in a scalp environment (pH = 5.5-8). Fig. 2i shows the FTIR spectra of FAL and MXD@FAL NPs. Three characteristic peaks at 3450, 2900 and 2850 cm^{-1} from amino stretching can be observed in

MXD@FAL NPs in comparison with FAL NPs, indicating the successful loading MXD. The characteristic peaks at 1750 and 1719 cm^{-1} can be contributed to the stretching vibrations of O-H and C-H alkane from VPA. These results are consistent with the characteristic peaks in composite paste (H-M/F/V), indicating no chemical interaction between the drugs and excipients (Fig. 2i).

3.2 Drug release and cytotoxicity *in vitro*

Loading efficiency and encapsulation percentage of MXD@FAL NPs are 24 ± 0.5 % and 82 ± 1 %, respectively. It implies that the composite paste L-M/F/V and H-M/F/V contain 0.024 g MXD and 0.096 g MXD, respectively. The results of the particle size distribution (Fig. 3a) show no obvious change after storage as solid at room temperature for 4 weeks, indicating good stability of MXD@FAL NPs. The spherical morphology of MXD@FAL NPs still can be maintained and no obvious change can be observed compared the initial structure of MXD@FAL NPs, implying the good stability of nanoparticles in the composite paste (Fig. 3b). The cumulative drug release behaviours *in vitro* are evaluated in PBS solution with pH = 5-7. As shown in Fig. 3c, a rapid drug release behaviour can be observed in the first 6 h culture for all samples. In a weak alkaline media, about 50% encapsulated drug can be released in 6 h, while cumulative drug release can be significantly improved due to the destruction of FAL NPs in a slightly acidic environment. More than 72% of the encapsulated drug can be released in the media with pH = 5. After 25 h culture, the cumulative drug release is close to 100%. It implies that the encapsulated MXD in MXD@FAL NPs can be released in the intra-scalp environment (pH = 5.5-8.0).

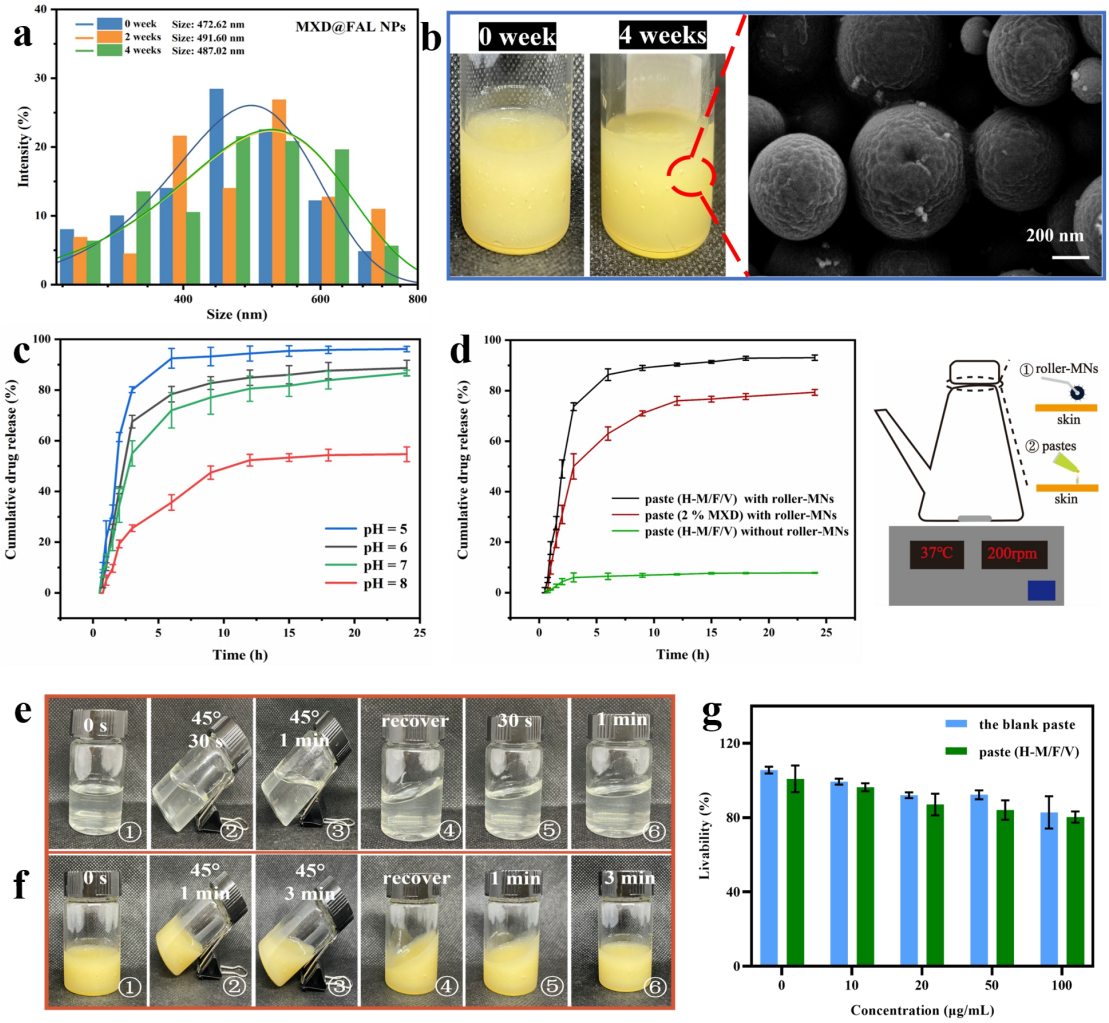

Fig. 3 The stability, drug release and cytotoxicity of MXD@FAL NPs. Particle size distribution (a) of MXD@FAL NPs from 0 to 4 weeks of storage at room temperature, storage stability of composite paste (H-M/F/V) (b), the release profile of MXD@FAL NPs in PBS with pH = 5-8 (c), the release profiles of H-M/F/V, 2 % MXD and H-M/F/V composite pastes without roller-MNs on artificial skin by a transdermal route *in vitro* (d), digital images of blank composite pastes (e) and H-M/F/V composite paste (f), and cell viability plots for blank and H-M/F/V composite pastes against L929 cells (g).

To simulate the drug delivery *in vivo*, a modified Franz diffusion cell is used to measure drug delivery efficiency by a transdermal delivery route. As shown in Fig. 3d, the composite paste containing 2 % MXD and the composite paste containing MXD@FAL NPs are spread on the roller-MNs pre-treated rat skin, respectively. The

cumulative drug of composite paste (2 % MXD) reaches ~ 91 % after culture for 24 h compared with ~ 78 % for composite paste loaded with MXD@FAL NPs, indicating the release of encapsulated drug can be can retarded due the barrier effect of drug carrier. In comparison with the drug release profile without roller-MNs on artificial skin, only less than ~10% cumulative drug release can be obtained after 24 h (Fig. S1). Therefore, the roller-MNs can create microchannels in the skin to accelerate drug delivery rate and enhance drug transdermal efficiency as well. In addition, the final formulation (2% MXD@FAL NPs with VA) still can maintain a good stability. The physical appearance and drug content in composite pastes have no signature changes after storage at 25±2 and 5±2 ºC for 3 months (Table S5). Fig. 3e shows the images of blank composite paste from vertical to inclined 45º states and it takes only 1 min to achieve the maximum deformation as well as the restoration. However, in the case of composite paste (H-M/F/V), it needs 3 min for deformation and restoration (Fig. 3f). The flexibility and poor mobility of the composite paste can afford better adhesion of the composite paste to the skin at various angles. It ensures adequate contact and administration on the scalp.

The cell viability against blank composite pastes is assessed by MTT. Fig. 3g shows the cell viability of L929 cells after co-culture for 24 h for the different concentrations of the blank composite paste leachate (20 μL/hole) that were obtained by soaking the blank composite paste in the DMEM for 24 h. The livability is more than 80 % even the leachate concentration increased to 100 μg/mL, indicating the excellent cytocompatibility of blank composite paste and biocompatibility of CMC

and HA. The cell survival of MXD@FAL NPs-loaded pastes (H-M/F/V) also has been assessed by MTT analysis. The livability is more than 80 % for the concentration ranging from 0 to 100 μg/mL, implying negligible effects after loading MXD@FAL NPs into composite pastes.

3.3 Hair regeneration evaluation

To estimate the efficacy of hair regeneration, androgenetic alopecia (AGA) models are first established. The skin on the back of the model mice exhibits pink and no hair regrowth showing that AGA models are effectively created after the 10-day-injection of dihydrotestosterone (DHT) [64]. Different administration strategies are performed on days 1, 5 and 9. Almost no hair is developed within 4 days in G1 (the blank group) due to the hair follicle (HF) cells in the resting period inhibited by DHT. The HF cells begin the anagen phase after 4 days and hair accelerates growth until to cover the naked sites. The effect of MXD and VPA on hair regrowth is evaluated by quantifying hair covered area (cm^2) over the dorsal skin area. On 4 days after administration, the hair growth in G2-G7 can be observed, covering approximately 15 % of the visible area. However, hair grows faster and denser in G4-G7 (Fig. 4b). It indicates the drugs (MXD and VPA) are in favour of hair regeneration. On 8 days after administration, G4-G7 groups show a higher hair coverage than G2 and G3 due to the promoting HF cells transformation from dormant to anagen phase by MXD and VPA. On 12 days after administration, all groups show hair regrowth in the alopecia area. However, the hair coverage in G2 and G3 groups is relatively lower compared with G4-G7 groups, further indicating that drugs are able

to promote hair regeneration. In addition, the naked edge areas in G4 and G5 groups still can be observed in comparison with the full coverage of regenerated hair in G6 and G7 groups. These results indicate MXD and VPA have a synergistic effect on hair regeneration.

Fig. 4c and 4d show the hair coverage for different groups during the administration period. G6 and G7 groups exhibit a higher hair coverage compared with other groups. In addition, with a higher concentration of MXD@FAL NPs in composite pastes, a relatively higher hair coverage can be observed compared with the lower-dose G6 group. Fig. 4e shows the hair density against different strategies after 12 days of administration. There are ~4,000 shafts/cm^2 for the healthy group after 12 days of natural growth. And only ~2,000 shafts/cm^2 for the roller-MNs and blank composite paste groups due to the inhibition of DHT. However, by loading MXD or VPA into composite pastes with the assistance of roller-MNs, the hair density can be increased to ~3,000 numbers/cm^2. It indicates that microchannels created by roller-MNs are favorable to transdermal delivery of MXD or VPA into the skin tissue. The adding VPA can compensate for the therapeutic effect caused by reducing MXD dosage. In addition, a significant synergistic effect on hair regeneration also can be observed after the incorporation of MXD@FAL NPs and VPA into composite pastes. The accelerated transition observed in G6 and G7 mice is due to increase expression of Wnt/β-catenin pathway. The hair density for G6 and G7 groups is ~4,000 numbers/cm^2 which is close to the healthy group, showing no significant difference between them.

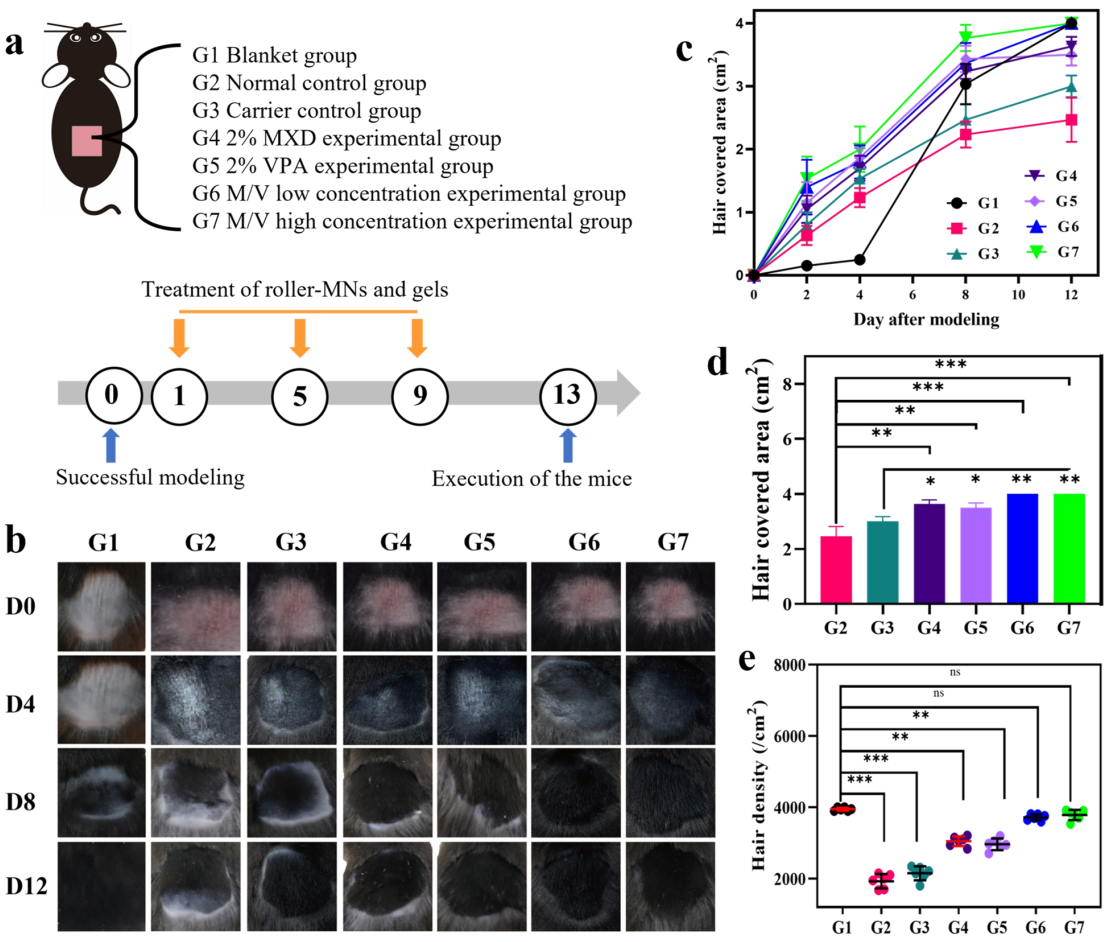

Fig. 4 Hair regeneration evaluation *in vivo*. Schematic representation of the establishment and the therapeutic strategies of the AGA mice (a), representative photographs (b), curves of changes in hair-covered areas on the back in G1-G7 (c), comparison of the area of dorsal hair coverage in G2/G3/G4/G5/G6/G7 on after 12 days administration (d), and hair follicle density (e) of mice hair regrowth status in G1-G7.

The effect of MXD and VPA on hair regrowth quality is evaluated by quantifying the length (mm) and diameters (μm) over the dorsal skin area. Interestingly, the AGA model mice only treated with roller-MNs also induced the growth of new hair, which may be induced by the mechanical stimulation of roller-MNs. Fig. 5a shows the average hair length after 12 days of administration. The average hair length of the G2 group is only ~1.01 mm, the shortest one in all groups. However, in the case of the G7 group, the average hair length of G7 is 2.24 mm, the longest in all tested groups. It

indicates that MXD and VPA work together to produce the most effective hair regeneration. The average hair diameter of the G2 group is 14.77 μm, the smallest in all groups in comparison with 23.12 μm of the G7 group (Fig. 5b). These results indicate that MXD and VPA not only promote the growth of hair but also improve the quality of regenerated hairs. The incorporation of MXD@FAL NPs into composite pastes can enhance the regrowth of HF cells by accelerating the telogen-to-anagen transition with a lower drug dose. In addition, the epidermal thicknesses in G1-G7 groups also have been tested after 12 days (Fig. S2). Among them, the G6, G7 and blanket group exhibit no significant differences in epidermal thickness. It indicated that the composite paste can promote hair regeneration without irreversible damage to skin.

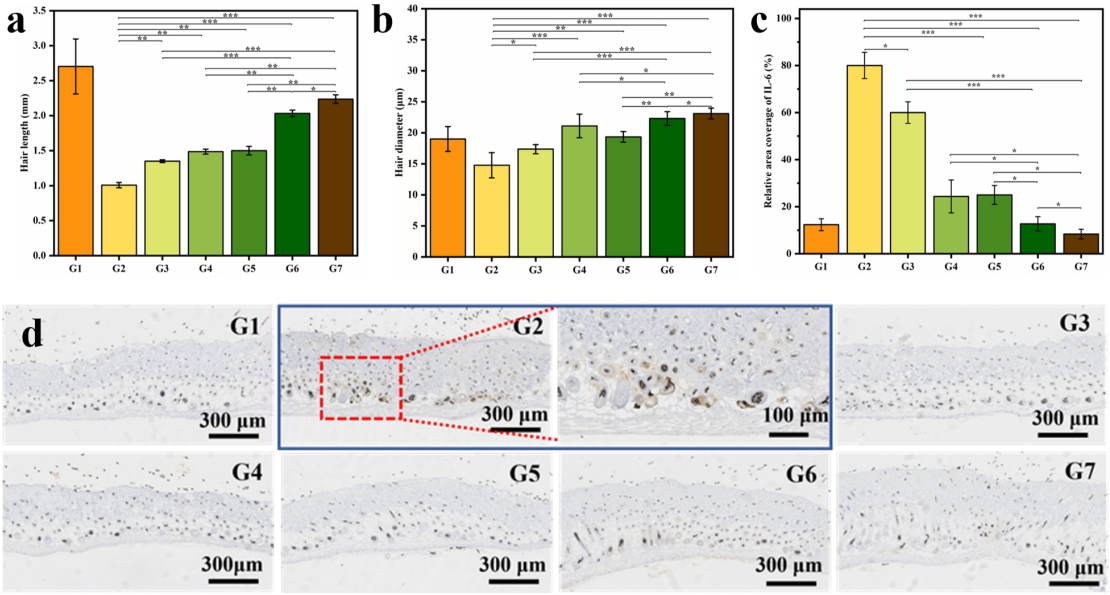

Fig. 5 Evaluation of hair regrowth quality and inflammatory factor *in vivo*. Comparison of hair length (a) hair diameter (b) and in G1-G7 after 12 days administration, quantitative analysis of IL-6 staining (c), and IL-6 staining images in G1-G7 groups (d).

The high expression of the inflammatory factor interleukin-6 (IL-6) inhibits the growth and proliferation of dermal papilla cells (DPC) [33], which inhibits hair

growth. Fig. 5c show that the highest secretion levels of IL-6 can be observed in G2 groups while a slight decrease of IL-6 in G3 groups after 12 days of administration. It may be contributed to emergency response to inflammation caused by mechanical insertion roller-MNs besides the induction of DHT [65-67]. However, a significant decrease in IL-6 expression can be obtained by the incorporation of FAL NPs, MXD and VPA into composite pastes, indicating that they can suppress the secretion of IL-6 and reduce the risk of inflammation as well. Fig. 5d shows the IL-6 staining images of hair-regenerated skin tissue after 12 days of administration. The G2 group exhibits the strongest IL-6 staining signals which is consistent with the analysis of IL-6 secretion levels.

Skin pigmentation will be occurred because of the formation of melanin by HFs cells during the transition of them from resting to anagen state [34,46,48,49]. Fig. 6a shows H&E staining images of hair-regenerated skin tissue after 12 days of administration. Only a small amount of HF cells can be observed in G2 and G3 groups. However, the large amount of HF cells can be founded after the incorporation of FAL NPs and VPA into composite pastes. Especially, in the case of G7 group, the most active HF cells can be obtained, indicating an earlier transition into anagen phase in all groups due to the synergistic effect of FAL NPs and VPA.

The ROS will be produced when the body is stimulated by oxidative stress which will inhibit hair growth due to the more vulnerable of HF cells to excessive ROS [59]. Fig. 6b shows ROS staining images of hair-regenerated skin tissue after 12 days of administration. The highest level of ROS can be observed in G2 group (Fig.

6c). It may be contributed to the inflammation stimulus-response caused by mechanical insertion roller-MNs. However, only low levels of ROS can be observed after the incorporation of FAL NPs, MXD and VPA into composite pastes. Especially, the ROS signal in G7 group is considerably lower than in other groups, showing the synergistic effect of FAL NPs and VPA to alleviate ROS secretion in the alopecia area. Based on the above results, CMC/HA/PVP composite pastes containing minoxidil-loaded nanoparticles and VPA exhibit excellent anti-inflammatory activity and hair growth promotion capacity, which have a potential application in the treatment of androgenetic alopecia.

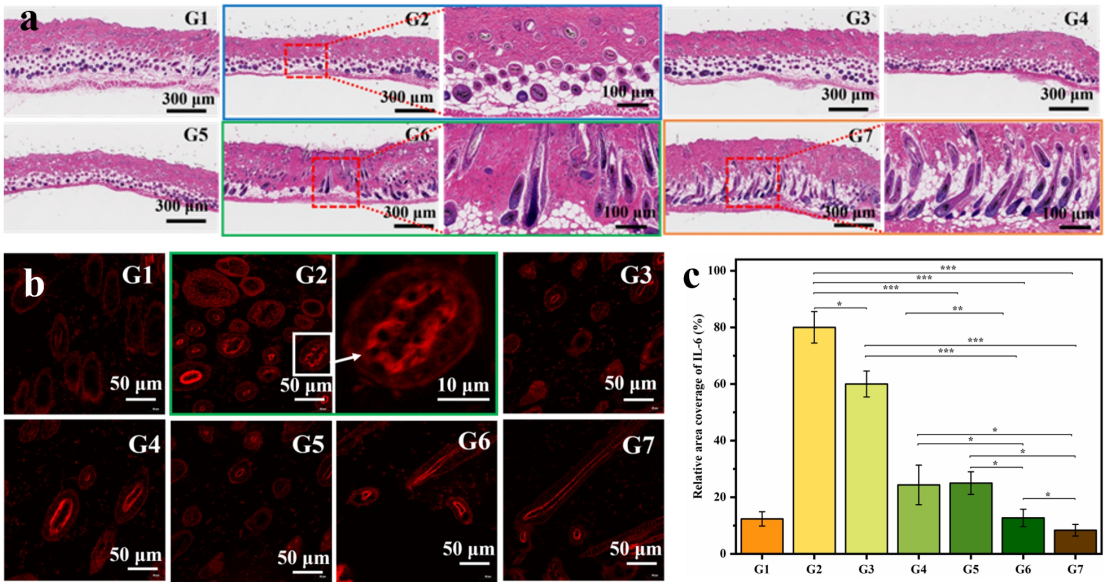

Fig. 6 Histological evaluation and ROS level expression. H&E staining (a) and ROS staining images (b) of hair regenerated skin tissue after 12 days administration, and quantitative analysis of ROS staining (c) in G1-G7 groups.

4. Conclusion

In this study, we designed CMC/HA/PVP composite pastes by incorporating minoxidil-loaded nanoparticles and VPA for the treatment of androgenetic alopecia. The lignin nanoparticles made from FA were effective for loading MXD, which can

scavenge ROS and decrease inflammation effectively. The excellent biocompatibility composite paste systems and the roller-MNs could create microchannels in the skin to enhance drug transdermal efficiency. In addition, the synergistic effect of FAL NPs, MXD and VPA could boost perifollicular vascularization, activate hair follicle stem cells, and reduce the dosage of minoxidil, showing a potential application in the treatment of androgenetic alopecia.

CRediT authorship contribution statement

Peixin Li: Resources, Investigation, Data curation, Formal analysis, Visualization, Writing original draft. **Yanfang Sun**: Resources, Data curation. **Lei Nie**: Validation, Writing-review & editing. **Amin Shavandi**: Validation, Writing-review & editing. **Khaydar E. Yunusov**: Validation, Writing-review & editing. **Yinjian Hua**: Resources, Data curation. **Guohua Jiang**: Methodology, Resources, Funding acquisitio, Validation, Writing-review & editing.

Declaration of competing interest

The authors declare that they have no known competing financial interests or personal relationships that could have appeared to influence the work reported in this paper.

Data availability

Data will be made available on request.

Acknowledgements

This work was supported by the Huadong Medicine Joint Funds of the Zhejiang Provincial Natural Science Foundation of China (LHDMZ23H300003) and National

Natural Science Foundation of China (51873194).

ORCID iDs

Guohua Jiang https://orcid.org/0000-0003-3666-8216

Lei Nie https://orcid.org/0000-0002-6175-5883

Amin Shavandi https://orcid.org/0000-0002-0188-3090

Khaydar E. Yunusov https://orcid.org/0000-0002-4646-7859

REFERENCES

[1] A.O. Adeniji, B.M. Twenter, M.C. Byrns, Y. Jin, M. Chen, J.D. Winkler, T.M. Penning, Development of potent and selective inhibitors of Aldo-keto reductase 1C3 (Type 5 17 beta-hydroxysteroid dehydrogenase) based on n-phenyl-aminobenzoates and their structure-activity relationships, J. Med. Chem 55 (2012) 2311-2323.

[2] M.J. Bertoli, R. Sadoughifar, R.A. Schwartz, T.M. Lotti, C.K. Janniger, Female pattern hair loss: a comprehensive review, Dermatol Ther. 33 (2020) 14055.

[3] J.M. Carnicle, A.J. Hendricks, V.Y. Shi, Reactivation of alopecia areata after dupilumab therapy for atopic dermatitis, Dermatitis. 32 (2021) E80-E82.

[4] M. Cepa, E.J.T. da Silva, G. Correia-Da-Silva, F.M.F. Roleira, N.A.A. Teixeira, Structure-activity relationships of new A, D-ring modified steroids as aromatase inhibitors: design, synthesis, and biological activity evaluation, J. Med. Chem. 48 (2005) 6379-6385.

[5] W. Deng, T. Hu, L. Han, B. Liu, X. Tang, H. Chen, X. Chen, M. Wan, miRNA microarray profiling in patients with androgenic alopecia and the effects of miR-133b on hair growth, Exp. Mol. Pathol. 118 (2021) 104589.

[6] A.G. Evans, J.M. Mwangi, R.W. Pope, M.G. Ivanic, M.A. Botros, G.E. Glassman, F.B. Pearce, Jr., S. Kassis, Platelet-rich plasma as a therapy for androgenic alopecia: a systematic review and meta-analysis, J Dermatolog Treat. 33 (2022) 498-511.

[7] S. Duarah, M. Sharma, J. Wen, Recent advances in microneedle-based drug delivery: special emphasis on its use in paediatric population, Eur. J. Pharm. Biopharm. 136 (2019) 48-69.

[8] D. Fu, J. Huang, K. Li, Y. Chen, Y. He, Y. Sun, Y. Guo, L. Du, Q. Qu, Y. Miao, Z. Hu, Dihydrotestosterone-induced hair regrowth inhibition by activating androgen receptor in

C57BL6 mice simulates androgenetic alopecia, Biomed. Pharmacother. 137 (2021) 111247.

[9] H. Galadari, S. Shivakumar, T. Lotti, U. Wollina, A. Goren, G.R. Rokni, S. Grabbe, M. Goldust, Low-level laser therapy and narrative review of other treatment modalities in androgenetic alopecia, Lasers Med. Sci. 35 (2020) 1239-1244.

[10] P. Gentile, L. Dionisi, J. Pizzicannella, B. de Angelis, D. de Fazio, S. Garcovich, A randomized blinded retrospective study: the combined use of micro-needling technique, low-level laser therapy and autologous non-activated platelet-rich plasma improves hair re-growth in patients with androgenic alopecia, Expert Opin. Biol. Ther. 20 (2020) 1099-1109.

[11] A.J. Bruce, T.P. Pincelli, M.G. Heckman, C.M. Desmond, J.R. Arthurs, N.N. Diehl, E.J. Douglass, C.J. Bruce, S.A. Shapiro, A randomized, controlled pilot trial comparing platelet-rich plasma to topical minoxidil foam for treatment of androgenic alopecia in women, Dermatol. Surg. 46 (2020) 826-832.

[12] P. Gentile, S. Garcovich, Systematic review of platelet-rich plasma use in androgenetic alopecia compared with minoxidil, finasteride, and adult stem cell-based therapy, Int. J. Mol. Sci. 21 (2020) 2702.

[13] R. Gonzalez-Louzao, C. Lucas-Abellan, H. Perez-Sanchez, J.P. Ceron-Carrasco, J.A. Gabaldon, S. Lopez-Miranda, M.J. Yanez-Gascon, M. Asin-Llorca, E. Nunez-Delicado, Encapsulation of finasteride with native and modified gamma-cyclodextrins. Extensive characterization of the complexes, Int. J. Pharm. 20 (2020) 587.

[14] A.F. Junqueira Ribeiro Pereira, T.O. de Almeida Coelho, Post-finasteride syndrome, An. Bras. Dermatol. 95 (2020) 271-277.

[15] P. Kochar, K. Nayak, S. Thakkar, S. Polaka, D. Khunt, M. Misra, Exploring the potential of minoxidil tretinoin liposomal based hydrogel for topical delivery in the treatment of androgenic alopecia, Cutan. Ocul. Toxicol. 39 (2020) 43-53.

[16] K. Saleem, B. Siddiqui, A.U. Rehman, M.M. Taqi, N. Ahmed, Exploiting recent trends in the treatment of androgenic alopecia through topical nanocarriers of minoxidil, Aaps Pharmscitech. 23 (2022) 292.

[17] R. Venkatesh, A. Pereira, K. Jain, N.K. Yadav, Minoxidil induced central serous chorioretinopathy treated with oral eplerenone - a case report, BMC Ophthalmol. 20 (2020) 219.

[18] Z. Lao, Y. Fan, Y. Huo, F. Liao, R. Zhang, B. Zhang, Z. Kong, H. Long, J. Xie, C. Sang, L. Fu, J. Lin, Y. Wu, L. Yu, G. Li, Physcion, a novel inhibitor of 5 alpha-reductase that promotes hair growth in vitro and in vivo, Arch. Dermatol. Res. 314 (2022) 41-51.

[19] I.G. Motofei, D.L. Rowland, M. Tampa, M.-I. Sarbu, M.-I. Mitran, C.-I. Mitran, A.P. Stoian, C.C. Diaconu, S. Paunica, S.R. Georgescu, Finasteride and androgenic alopecia; from therapeutic options to medical implications, J Dermatolog Treat. 31 (2020) 415-421.

[20] T. Searle, F.R. Ali, F. Al-Niaimi, The versatility of azelaic acid in dermatology, J Dermatolog Treat. 33 (2022) 722-732.

[21] Y.J. Tak, S.Y. Lee, A.R. Cho, Y.S. Kim, A randomized, double-blind, vehicle-controlled clinical study of hair regeneration using adipose-derived stem cell constituent extract in androgenetic alopecia, Stem Cells Transl Med. 9 (2020) 839-849.

[22] C. Wei, P. Bovonratwet, A. Gu, G. Moawad, J.I. Silverberg, A.J. Friedman, Spironolactone use does not increase the risk of female breast cancer recurrence: a retrospective analysis, J.

Am. Acad. Dermatol. 83 (2020) 1021-1027.

[23] X. Zhang, D. Zhou, T. Ma, Q. Liu, Vascular endothelial growth factor protects CD200-rich and CD34-positive hair follicle stem cells against androgen-induced apoptosis through the phosphoinositide 3-Kinase/Akt pathway in patients with androgenic alopecia, Dermatol. Surg. 46 (2020) 358-368.

[24] S.F. Lahiji, S.H. Seo, S. Kim, M. Dangol, J. Shim, C.G. Li, Y. Ma, C. Lee, G. Kang, H. Yang, K.-Y. Choi, H. Jung, Transcutaneous implantation of valproic acid-encapsulated dissolving microneedles induces hair regrowth, Biomaterials. 167 (2018) 69-79.

[25] S.J. Jo, H. Shin, Y.W. Park, S.H. Paik, W.S. Park, Y.S. Jeong, H.J. Shin, O. Kwon, Topical valproic acid increases the hair count in male patients with androgenetic alopecia: a randomized, comparative, clinical feasibility study using phototrichogram analysis, J. Dermatol. 41 (2014) 285-291.

[26] M. Zhu, D. Kong, R. Tian, M. Pang, M. Mo, Y. Chen, G. Yang, H.L. Cheng, X. Lei, K. Fang, B. Cheng, Y. Wu, Platelet sonicates activate hair follicle stem cells and mediate enhanced hair follicle regeneration, J. Cell. Mol. Med. 24 (2020) 1786-1794.

[27] C.C. Zouboulis, K. Degitz, Androgen action on human skin from basic research to clinical significance, Exp. Dermatol. 13 (2004) 5-10.

[28] G.E. Glass, Photobiomodulation: The clinical applications of low-level light therapy, Aesthet. Surg. J. 41 (2021) 723-738.

[29] J. Griggs, B. Burroway, A. Tosti, Pediatric androgenetic alopecia: a review, J. Am. Acad. Dermatol. 85 (2021) 1267-1273.

[30] Y. Gu, Q. Bian, Y. Zhou, Q. Huang, J. Gao, Hair follicle-targeting drug delivery strategies for

the management of hair follicle-associated disorders, Asian J Pharm Sci. 17 (2022) 333-352.

[31] J.-H. Fang, C.-H. Liu, R.-S. Hsu, Y.-Y. Chen, W.-H. Chiang, H.-M.D. Wang, S.-H. Hu, Transdermal composite microneedle composed of mesoporous iron oxide nanoraspberry and PVA for androgenetic alopecia treatment, Polymers. 12 (2020) 1392.

[32] R. Krysiak, K. Kowalcze, B. Okopien, Impaired metabolic effects of metformin in men with early-onset androgenic alopecia, Pharm. Rep. 74 (2022) 216-228.

[33] M.H. Kwack, C.H. Seo, P. Gangadaran, B.-C. Ahn, M.K. Kim, J.C. Kim, Y.K. Sung, Exosomes derived from human dermal papilla cells promote hair growth in cultured human hair follicles and augment the hair-inductive capacity of cultured dermal papilla spheres, Exp. Dermatol. 28 (2019) 854-857.

[34] H.A. Oh, J. Kwak, B.J. Kim, H.J. Jin, W.S. Park, S.J. Choi, W. Oh, S. Um, Migration inhibitory factor in conditioned medium from human umbilical cord blood-derived mesenchymal stromal cells stimulates hair growth, Cells. 9 (2020) 1344.

[35] A.C.S. Oliveira, P.M. Oliveira, M. Cunha-Filho, T. Gratieri, G.M. Gelfuso, Latanoprost loaded in polymeric manocapsules for effective topical teatment of alopecia, Aaps Pharmscitech. 21 (2020) 305.

[36] H. Wang, Y. Fu, J. Mao, H. Jiang, S. Du, P. Liu, J. Tao, L. Zhang, J. Zhu, Strong and tough supramolecular microneedle patches with ultrafast dissolution and rapid-onset capabilities, Adv. Mater. 34 (2022) 2207832.

[37] P. Liu, Y. Fu, F. Wei, T. Ma, J. Ren, Z. Xie, S. Wang, J. Zhu, L. Zhang, J. Tao, J. Zhu, Microneedle patches with O-2 propellant for deeply and fast delivering photosensitizers: towards improved photodynamic therapy, Adv. Sci. 9 (2022) 2202591.

[38] P. Liu, H. Du, Z. Wu, H. Wang, J. Tao, L. Zhang, J. Zhu, Hydrophilic and anti-adhesive modification of porous polymer microneedles for rapid dermal interstitial fluid extraction, J. Mater. Chem. B 9 (2021) 5476-5483.

[39] T. Liu, Y. Sun, G. Jiang, W. Zhang, R. Wang, L. Nie, A. Shavandi, K.E. Yunusov, U.E. Aharodnikau, S.O. Solomevich, Porcupine-inspired microneedles coupled with an adhesive back patching as dressing for accelerating diabetic wound healing, Acta Biomater. 160 (2023) 32-44.

[40] R. Wang, G. Jiang, U.E. Aharodnikau, K. Yunusov, Y. Sun, T. Liu, S.O. Solomevich, Recent advances in polymer microneedles for drug transdermal delivery: design strategies and applications, Macromol. Rapid Commun. 43 (2022) 2200037.

[41] Z. Zeng, G. Jiang, Y. Sun, U.E. Aharodnikau, K.E. Yunusov, X. Gao, T. Liu, S.O. Solomevich, Rational design of flexible microneedles coupled with CaO_2@PDA-loaded nanofiber films for skin wound healing on diabetic rats, Biomater Sci. 10 (2022) 5326-5339.

[42] L. Siddiqui, J. Bag, D. Mittal, A. Leekha, H. Mishra, M. Mishra, A.K. Verma, P.K. Mishra, A. Ekielski, Z. Iqbal, S. Talegaonkar, Assessing the potential of lignin nanoparticles as drug carrier: synthesis, cytotoxicity and genotoxicity studies, Int. J. Biol. Macromol. 152 (2020) 786-802.

[43] R. C. Sun, Lignin source and structural characterization, Chemsuschem 13 (2020) 4385-4393.

[44] S. Zhang, Y. Chen, Z. Liu, Z. Zhao, Advances in lignin valorization from a biorefinery concept, Chin J Biotechnol. 37 (2021) 3108-3128.

[45] C. Zhao, J. Yang, M. Chen, W. Chen, X. Yang, H. Ye, L. Wang, Y. Wang, J. Shi, F. Yue, X. Ma, Synthetic lignin-derived therapeutic nano reagent as intestinal pH-sensitive drug carriers

capable of bypassing the gastric acid environment for colitis treatment, Acs Nano. (2022) 811-824.

[46] D.H. Marks, L.R. Penzi, E. Ibler, A. Manatis-Lornell, D. Hagigeorges, M. Yasuda, L.A. Drake, M.M. Senna, The medical and psychosocial associations of alopecia: recognizing hair loss as more than a cosmetic concern, Am. J. Clin. Dermatol. 20 (2019) 195-200.

[47] A. Martinez-Lopez, T. Montero-Vilchez, A. Sierra-Sanchez, A. Molina-Leyva, S. Arias-Santiago, Advanced medical therapies in the management of non-scarring alopecia: areata and androgenic alopecia, Int. J. Mol. Sci. 21 (2020) 8390.

[48] H. Morinaga, Y. Mohri, M. Grachtchouk, K. Asakawa, H. Matsumura, M. Oshima, N. Takayama, T. Kato, Y. Nishimori, Y. Sorimachi, K. Takubo, T. Suganami, A. Iwama, Y. Iwakura, A.A. Dlugosz, E.K. Nishimura, Obesity accelerates hair thinning by stem cell-centric converging mechanisms, Nature. 595 (2021) 266.

[49] S. Paul, I. Licona-Vazquez, F.I. Serrano-Cano, N. Frias-Reid, C. Pacheco-Dorantes, S. Pathak, S. Chakraborty, A. Srivastava, Current insight into the functions of microRNAs in common human hair loss disorders: a mini review, Hum. Cell. 34 (2021) 1040-1050.

[50] M. Roohaninasab, A. Goodarzi, M. Ghassemi, A. Sadeghzadeh-Bazargan, E. Behrangi, N. Najar Nobari, Systematic review of platelet-rich plasma in treating alopecia: focusing on efficacy, safety, and therapeutic durability, Dermatol Ther. 34 (2021) 14768.

[51] J.-Y. Ryu, E.-J. Won, H.A.R. Lee, J.H. Kim, E. Hui, H.P. Kim, T.-J. Yoon, Ultrasound-activated particles as CRISPR/Cas9 delivery system for androgenic alopecia therapy, Biomaterials. 232 (2020) 119736.

[52] G. Shamloul, A. Khachemoune, An updated review of the sebaceous gland and its role in

health and diseases Part 2: pathophysiological clinical disorders of sebaceous glands.

[53] A.N. Sharma, L. Michelle, M. Juhasz, P. Muller Ramos, N. Atanaskova Mesinkovska, Low-dose oral minoxidil as treatment for non-scarring alopecia: a systematic review, Int. J. Dermatol. 59 (2020) 1013-1019.

[54] A.J. Paredes, F. Volpe-Zanutto, A.D. Permana, A.J. Murphy, C.J. Picco, L.K. Vora, J.A. Coulter, R.F. Donnelly, Novel tip-loaded dissolving and implantable microneedle array patches for sustained release of finasteride, Int. J. Pharm. 606 (2021) 120885.

[55] K. Prabahar, U. Udhumansha, N. Elsherbiny, M. Qushawy, Microneedle mediated transdermal delivery of beta-sitosterol loaded nanostructured lipid nanoparticles for androgenic alopecia, Drug Deliv. 29 (2022) 3022-3034.

[56] S. Ruan, Y. Zhang, N. Feng, Microneedle-mediated transdermal nano delivery systems: a review, Biomater Sci. 9 (2021) 8065-8089.

[57] G. Yang, G. Chen, Z. Gu, Transdermal drug delivery for hair regrowth, Mol. Pharm. 18 (2021) 483-490.

[58] G. Yang, Q. Chen, D. Wen, Z. Chen, J. Wang, G. Chen, Z. Wang, X. Zhang, Y. Zhang, Q. Hu, L. Zhang, Z. Gu, A therapeutic microneedle patch made from hair-derived keratin for promoting hair regrowth, Acs Nano. 13 (2019) 4354-4360.

[59] A. Yuan, F. Xia, Q. Bian, H. Wu, Y. Gu, T. Wang, R. Wang, L. Huang, Q. Huang, Y. Rao, D. Ling, F. Li, J. Gao, Ceria nanozyme-integrated microneedles reshape the perifollicular microenvironment for androgenetic alopecia treatment, Acs Nano. 15 (2021) 13759-13769.

[60] K. Prabahar, U. Uthumansha, N. Elsherbiny, M. Qushawy, Enhanced skin permeation and controlled release of β-sitosterol using cubosomes encrusted with dissolving microneedles

for the management of alopecia, Pharm. 16 (2023) 563.

[61] K. Prabahar, U. Udhumansha, N. Elsherbiny, M. Qushawy, Microneedle mediated transdermal delivery of β-sitosterol loaded nanostructured lipid nanoparticles for androgenic alopecia, Drug Deliv. 29 (2022) 3022-3034.

[62] L. Chen, S.-M. Luo, C.-M. Huo, Y.-F. Shi, J. Feng, J.-Y. Zhu, W. Xue, X. Qiu, New insight into lignin aggregation guiding efficient synthesis and functionalization of a lignin nanosphere with excellent performance, Green Chem. 24 (2022) 285-294.

[63] W. Zhao, L.-P. Xiao, G. Song, R.-C. Sun, L. He, S. Singh, B.A. Simmons, G. Cheng, From lignin subunits to aggregates: insights into lignin solubilization, Green Chem. 19 (2017) 3272-3281.

[64] J.H. Upton, R.F. Hannen, A.W. Bahta, N. Farjo, B. Farjo, M.P. Philpott, Oxidative stress-associated senescence in dermal papilla cells of men with androgenetic alopecia, J. Invest. Dermatol. 135 (2015) 1244-1252.

[65] P.F. Li, L.M. Ruan, G.H. Jiang, Y.F. Sun, R.F. Wang, X.F. Gao, K.E. Yunusov, U.E. Aharodnikau, S.O. Solomevich, Design of 3D polycaprolactone/ epsilon-polylysine-modified chitosan fibrous scaffolds with incorporation of bioactive factors for accelerating wound healing, Acta Biomater. 152 (2022) 197-209.

[66] R. Wang, H. Wang, G.H. Jiang, Y.F. Sun, T.Q. Liu, L. Nie, A. Shavandi, K.E. Yunusov, U.E. Aharodnikau, S.O. Solomevich, Transdermal delivery of allopurinol to acute hyperuricemic mice via polymer microneedles for the regulation of serum uric acid levels, Biomater Sci. 11 (2023) 1704-1713.

[67] M.J. Feng, G.H. Jiang, Y.F. Sun, U.E. Aharodnikau, K.E. Yunusov, T.Q. Liu, Z.Y. Zeng, S.O.

Solomevich, Integration of metformin-loaded mesoporous bioactive glass nanoparticles and free metformin into polymer microneedles for transdermal delivery on diabetic rats, Inorg. Chem. Commun. 144 (2022) 109896.